crystals

MDPI

Article

Biosynthesis of Silver Nanoparticles Using *Bersama engleriana* Fruits Extracts and Their Potential Inhibitory Effect on Resistant Bacteria

Michele Stella Majoumouo [1,2], Marius Belmondo Tincho [2,3,*], Youmbi Diane Yimta [1], Tayo Alex Adekiya [4], Raphael Taiwo Aruleba [5], Nimibofa Ayawei [6], Fabrice Fekam Boyom [1] and Thureyah Morris [7]

1 Antimicrobial & Biocontrol Agents Unit, Laboratory for Phytobiochemistry and Medicinal Plants Studies, Department of Biochemistry, University of Yaoundé 1, Yaoundé PO. Box 812, Cameroon; 3770612@myuwc.ac.za (M.S.M.); youmbi_diane@yahoo.fr (Y.D.Y.); ffefe@yahoo.com (F.F.B.)
2 Department of Biotechnology, Faculty of Natural Sciences, University of the Western Cape, Private Bag X17, Bellville 7535, South Africa
3 Department of Biochemistry and Molecular Biology, Faculty of Science, University of Buea, Buea P.O. Box 63, Cameroon
4 Department of Pharmaceutical Sciences, Howard University, Washington, DC 20059, USA; adekiyatalex@gmail.com
5 Department of Molecular and Cell Biology, Faculty of Science, University of Cape Town, Cape Town 7701, South Africa; arulebataiwo@yahoo.com
6 Department of Chemistry, Bayelsa Medical University, Yenagoa PMB 178, Nigeria; ayawei4acad@gmail.com
7 Department of Medical Bioscience, Faculty of Natural Sciences, University of the Western Cape, Private Bag X17, Bellville 7535, South Africa; tmorris@uwc.ac.za
* Correspondence: 3173772@myuwc.ac.za

Abstract: The absence of novel, safe, and effective bactericide is an urgent concern worldwide and remains a challenge in scientific communities. The unique proprieties of silver nanoparticles (SNPs) synthesized from plant extracts make them a suitable candidate to overcome these limitations. Herein, we synthesized SNPs from *Bersama engleriana* fruit (BEfr) extracts and determined their potential antibacterial activity and mode of action. SNPs were synthesized from BEfr methanolic fruit extracts at 25 and 70 °C, and the antibacterial effectiveness of SNPs against bacterial strains was investigated. The surface plasmon resonance peaked at 430.18 and 434.08 nm, respectively, for SNPs synthesized at 25 and 70 °C, confirming SNPs synthesis. BEfr-SNPs had minimum inhibitory concentrations (MIC) range of 0.234 to >50 µg/mL, which was 30-fold greater than extract alone (MIC of 500 µg/mL). BEfr-SNPs-25 °C was potent against six bacterial strains (*S. aureus*, *S. enterica*, *MRS. aureus*, *K. pneumonia*, and *S. pyogenes*), with MIC range of 0.339 to 6.25 µg/mL. The mode of action of BEfr-SNPs-25 °C was achieved by an *MRSA* bacteria strain outer membrane and DNA nucleotide linkage. These results suggest that our synthesized SNPs, especially BEfr-SNPs-25 °C, demonstrated an enhanced antibacterial effect and could be potential candidates for bacterial infection treatment.

Keywords: green nanotechnology; *Bersama engleriana*; antibacterial activity; mode of action

Citation: Majoumouo, M.S.; Tincho, M.B.; Yimta, Y.D.; Adekiya, T.A.; Aruleba, R.T.; Ayawei, N.; Boyom, F.F.; Morris, T. Biosynthesis of Silver Nanoparticles Using *Bersama engleriana* Fruits Extracts and Their Potential Inhibitory Effect on Resistant Bacteria. *Crystals* **2022**, *12*, 1010. https://doi.org/10.3390/cryst12071010

Academic Editor: Jaime Gómez Morales

Received: 13 June 2022
Accepted: 14 July 2022
Published: 21 July 2022

1. Introduction

Infectious diseases are a severe and persistent public-health issue affecting millions around the world and account for one-quarter to one-third of all death cases across the globe. In African countries, infectious diseases have a serious influence on the social security and economic output throughout the Africa continent [1]. Despite advances in pharmaceutical research, rates of infectious diseases are increasing globally as a result of human behaviour, denser and larger cities, an increase in commercial activities and travel/immigration, inappropriate antibiotic usage, and the advent of drug-resistant organisms.

Multidrug-resistant (MDR) bacteria continue to be one of the most difficult problems in public health care [2]. According to the Centers for Disease Control and Prevention

(CDC) report, approximately 2.8 million individuals are afflicted with antibiotic-resistant bacteria, with over 35,000 deaths annually [3]. Bacterial pathogens, such as *Pseudomonas aeruginosa*, *Salmonella enterica*, *Klebsiella pneumoniae*, *Escherichia coli*, *Streptococcus pneumonia*, and Methicillin-resistant *Staphylococcus aureus* (*MRSA*), have been identified as primary causative agents for skin infections, infections of the lungs, as well as other serious diseases [4]. Due to antibiotic resistance, the treatment of these infections is becoming more difficult. Consequently, these antibiotic-resistant bacteria are the primary cause of nosocomial infections globally. The number of diseases caused by these resistant strains is growing, and bacteria have developed several mechanisms to become antimicrobials resistant [5]. Some strategies employed by pathogenic bacteria include the inactivation of enzymes, decrease in cell permeability, target overproduction, target protection, change in target enzyme/site, and increase in efflux as a result of efflux pump overexpression [6]. Many other complex phenotypes, for example, the formation of biofilm and quorum sensing, do not occur due to antibiotic exposure, despite the fact that biofilm growth can be activated by antibiotics and hence result in tolerance [6]. To overcome this and other forms of resistance, several techniques, such as the application of structural nanomaterial, are now being explored.

Recent developments in nanotechnology-based therapies have created a novel golden opportunity for slowing down the increase of multidrug resistance in microorganisms [7]. The application of nanomaterials, particularly silver nanoparticles (SNPs), has demonstrated promising and tremendous uses in wound-healing, drug delivery, bio-labelling, cosmetics, water purification, and food preservation [8]. Moreover, SNPs have gained a lot of interest from scientific communities as a potent antibacterial agent.

Several conventional approaches have been employed for decades to synthesize SNPs. For example, physical techniques like laser ablation, melt mixing, sputtering, and physical vapour deposition, as well as chemical techniques, such as thermolysis, microemulsion, sol-gel, and photoreduction. These methods usually lead to nanoparticle volatility, toxic chemical adhesion on the nanoparticles surface, and the production of hazardous by-products [9]. Thus, green silver nanoparticle synthesis represents a new sustainable method for nanoparticle production and to design alternative energy-efficient, non-toxic, and environmentally friendly techniques [10]. The use of plants for nanoparticles synthesis has several advantages over other biological synthesis techniques since it eliminates the need for cell culture maintenance and integrates support for the synthesis of large-scale nanoparticle [11]. The green synthesis of SNPs from plant extracts (a) provides stable nanoparticles synthesis; (b) enables biocompatible functionalization on the nanoparticle surface, providing a more active surface area for physiological environment interactions; (c) formation of no hazardous byproduct; and (d) requires no stabilizing agents or additional reduction, which result in a more cost-effective procedure [9,12]. A study showed that SNPs synthesized in an environmentally friendly approach from the leaf extracts of *Argemone mexicana* with a particle size of 20 nm demonstrated antifungal and antimicrobial effect against a number of fungal and bacterial microorganisms [13]. Additionally, 11 nm size SNPs synthesized from leaf extracts of *Terminalia mantaly*, showed significant antibacterial activities against several bacterial strains (*Streptococcus pneumoniae*, *Kbesiella pneumoniae*, *Haemophilus influenzae*, *Shigella flexneri*, *Salmonela enterica*, and *Staphylococcus aureus*) [7].

While the actual mechanism of SNPs antibacterial activity is still not completely understood, and some remain to be clarified, it has, however, been fully proven that nanosilver accumulates at the surface of bacterial membranes and penetrates the cell walls of the bacteria, thereby resulting in their destabilization, change in cell membrane structure, and even cell death [14]. Additionally, previous reports have stated that the inhibitory effect of SNPs can be ascribed to the electrostatic interaction found within the negative charge on the bacterial cells and the positive charge of nanoparticles [15]. In addition, it has been postulated that nano silver-based systems exhibit their antibacterial actions via the following mechanisms: (a) the destruction of the microbial membrane, which is caused by the directed physicochemical linkage of SNPs on the surface of the cell, and consequent

functional and structural modifications (such as membrane destabilization, formation of gap, cytoplasm leakage, and piercing of membrane); and (b) damage to microbial subcellular structures induced by releasing the free Ag^+ ions and the resultant production of reactive oxygen species (ROS) or inactivation of important macromolecules (proteins, enzymes, and nucleotides) [16]. Hence, the current study aims to develop a green technique for silver nanoparticle synthesis from the fruit extracts of the plant *Bersama engleriana* (BEfr-SNPs). We also investigated the possible modes of action, including the time-kill kinetic growth inhibition, the effect of BEfr-SNPs on the outer membrane destabilization, and DNA nucleotide linkage.

2. Results and Discussion

2.1. Green Synthesis and UV–Visible Spectroscopy Evaluation

After 24 h of incubation in a silver nitrate ($AgNO_3$) aqueous solution, the fresh fruit extract of *Bersama engleriana* became a dark yellowish and brownish colour (Figure 1), indicating that phytochemicals reduced silver ions to SNPs. The dark brown colour was obtained for BEfr-SNPs produced at 70 °C. The variation in colour depended on the temperature at which the SNPs were synthesized and the concentration of the extracts [7]. SNPs have distinct optical characteristics that significantly interact with specific wavelengths of light, which result in a distinctive peak between 400 and 450 nm for surface plasmon resonance (SPR) [8]. Basically, the absorption peak of SPR occurs primarily in metal nanoparticles. As a result, the presence of an SPR peak is the key indicator of formation of metal nanoparticle. SPR peak is critical in the synthesis of nanoparticle to regulate not just particle size but also morphology and particle shape [17]. Interestingly, in our study, SPR peaks were 430.18 and 434.08 nm (Figure 1) for synthesized BEfr-SNPs at 25 °C and 70 °C, respectively, which confirm the formation of SNPs. These results were supported by similar findings obtained in a study performed by Dakshayani et al., 2019 [18], where the formation of SNPs SPR peaks was monitored at 430 nm.

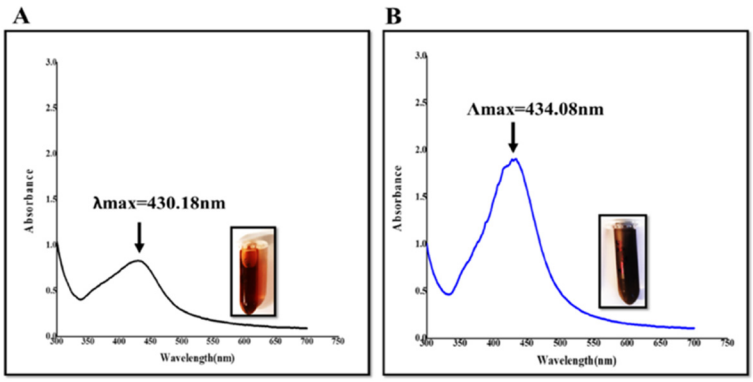

Figure 1. Colour change and the profiles of UV–vis spectral of BEfr-SNPs synthesized at 25 °C and 70 °C. (**A**) silver nanoparticles synthesized at 25 °C; (**B**): silver nanoparticles synthesized at 70 °C. Abbreviations: BEfr: Fruits extracts from methanolic of *Bersama engleriana*; BEfr-SNPs: BEfr silver nanoparticles.

2.2. Full Characterization of BEfr-SNPs

2.2.1. Dynamic Light Scattering (DLS) Evaluation

The DLS was used to estimate the average hydrodynamic diameter, polydispersity index (Pdi), as well as zeta potential parameters of the BEfr-SNPs (Figures 2 and 3 and Table 1). The sizes of BEfr-SNPs differed based on the temperature (25 °C and 70 °C) in which the synthesis was carried out. The average hydrodynamic size of 51.31 and 48.06 nm was obtained for synthesized BEfr-SNPs at 25 °C and 70 °C, respectively. Zeta potential results showed that the synthesized BEfr-SNPs is negatively charged with potential values of −17.30 and −20.83 mV for BEfr-SNPs-25 °C and BEfr-SNPs-70 °C, respectively. The most reliable zeta potential value for most nanosuspensions was approximately ±30 mV; the val-

ues of zeta potential generated from this study are within this range [19]. However, using the Zetasizer Malvern, the quality of the results was revealed to be good (Figures 2 and 3). Generally, SNPs that present negative values of zeta potential indicate that there are significant repulsion forces between the SNPs that prohibit NPs aggregation and agglomeration in solution [20]. The polydispersity index (PDI) revealed that all synthesized SNPs had a narrow size distribution, as demonstrated by a PDI value of 0.48 and 0.66 for BEfr-SNPs-25 °C and BEfr-SNPs-70 °C, respectively. Based on the International Organization for Standardization (ISO), values of PDI greater than 0.7 imply that the samples possess a great wide range of size distribution. In contrast, values of PDI less than or equal to 0.5 suggest that the samples are more monodispersed. Hence, the nanoparticles from BEfr-SNPs-25 °C were monodisperse, while those from BEfr-SNPs-70 °C were polydisperse. These findings clearly demonstrated that the nanoparticles synthesized have a negatively charged surface and a narrow size distribution.

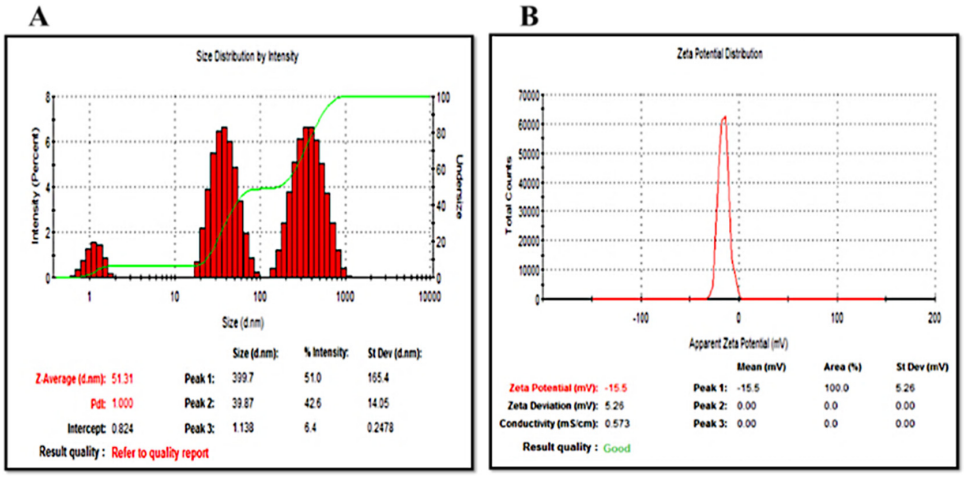

Figure 2. Dynamic light characterization of biosynthesized BEfr-SNPs-25 °C. (**A**) Size distribution of particles with average size intensity of 51.31 nm and (**B**) the distribution of zeta potential with a maximum charge of −15.5 mV. All data are presented as means SD (n = 3).

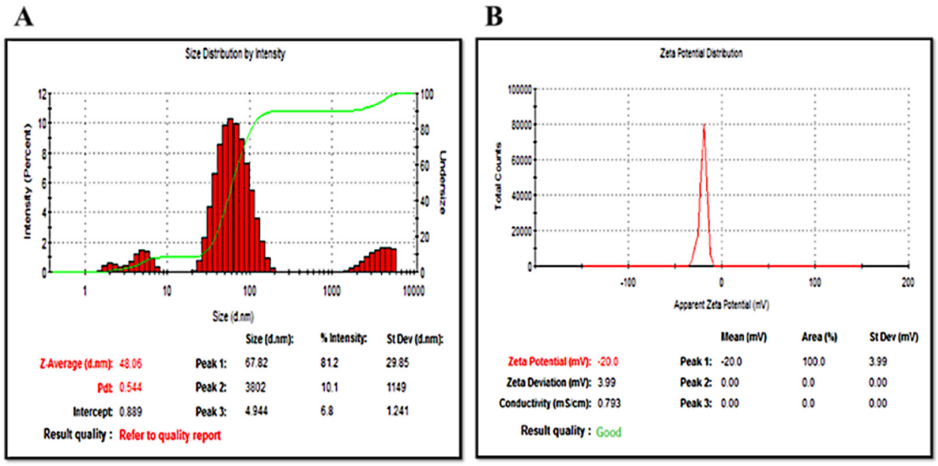

Figure 3. Dynamic light characterization of biosynthesized BEfr-SNPs-70 °C. (**A**) Size distribution of particles with average size intensity of 48.06 nm and (**B**) the distribution of zeta potential with a maximum charge of −20 mM. All data are presented as means SD (n = 3).

Table 1. Surface plasmon resonance and dynamic light scattering parameters of BEfr-SNPs.

Codes	Dynamic Light Scattering Parameters					
	Optimum Concentration (mg/mL)	λmax (nm)	Average Diameter (nm)	Average Zeta Potential (mV)	Deviation/Conductivity (ms/cm)	Pdi
BeFr-SNPs-25 °C	0.39	434.08	51.31	−17.30 ± 1.28	5.26/0.573	0.480
BeFr-SNP-70 °C	0.78	430.18	48.06	−20.83 ± 0.59	7.40/10.788	0.665

2.2.2. HRTEM Characterization of BEfr-SNPs

The nanostructure morphology of BEfr-SNPs was elucidated using an HRTEM microscope, and the TEM micrograph images showed several geometrical shapes (Figure 4). The silver nanoparticles produced at 25 °C were mostly spherical and most were well dispersed. The great distribution of SNPs with a small particle size obtained may be ascribed to the bio-components of *Bersama engleriana*, which play both reductants roles for Ag ions as well as a stabilizing agent for the synthesized SNPs [21]. The monodispersity of SNPs is an indication that SNPs are bounded using the layer of organic molecule, this suggests that particular adhering/capping phytochemical agents present in *Bersama engleriana* extract are involved in the SNPs biosynthesis procedure [22]. However, the mixture of geometric shapes, such as triangular, rectangular and spherical, was obtained with silver nanoparticles produced at 70 °C. These anisotropic shapes obtained in SNPs synthesized at 70 °C could be attributed to the capping and reducing phytochemicals that enabled thermodynamic stability and not only that but also defined the NPs bioactivities [7,23]. Many reports have demonstrated that SNPs with different geometrical shapes are usually common to NPs synthesized via the plant-facilitated synthesis [7,17]. This postulation may be due to different phytochemicals present in the extracts, which could act as a synergy to the reduction of the ions and produce SNPs [24]. It has been described that polyphenols generate NPs with different kinds of shapes [25]. Biomolecules with strongly polar groups (for instance, -OH) on their surfaces could accelerate nucleation and cause SNP formation. Based on the HRTEM analysis, silver nanoparticles produced at 70 °C appear to be agglomerated. Interestingly, the HRTEM micrograph images of the synthesized SPNs both at 25 °C and 70 °C supported the average particle size revealed in the DLS evaluation; this excellent result could be attributed to the standard absorption peak observed in the SPR evaluation.

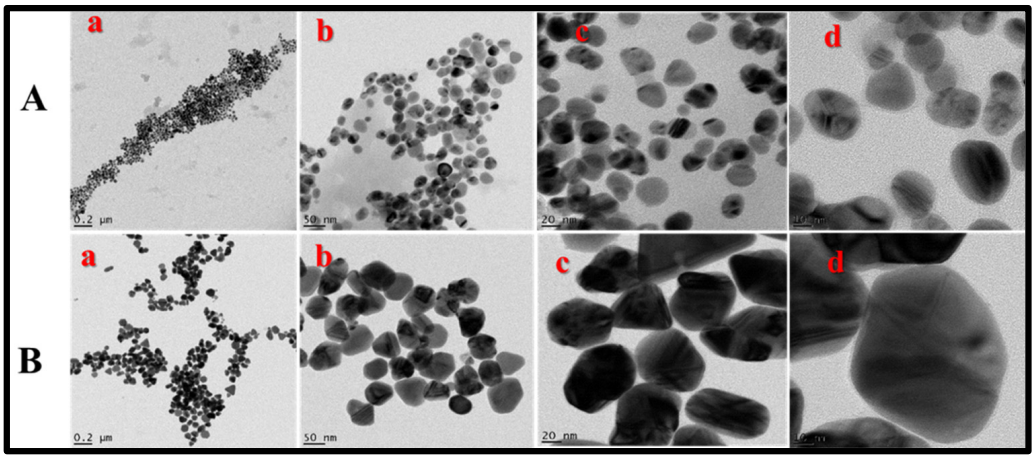

Figure 4. HRTEM micrographs patterns of BEfr-SNPs. (**A**): BEfr-SNPs-25 °C; (**B**): BEfr-SNPs-70 °C; (**a**): 0.2 µm; (**b**): 50 nm; (**c**): 20 nm; (**d**): 10 nm. Abbreviations: SAED: selected area electron diffraction; TEM: Transmission election microscope.

2.2.3. Size Distribution Frequency and Selected Area Diffraction Pattern

The nanocrystalline nature and size distribution of the synthesized SNPs were identified through image G (Figure 5g,h) and selected area diffraction pattern (Figure 5c,d) that are among the components of HRTEM analysis. Regarding the SAED pattern, SNPs exhibited four intense Bragg's reflection peaks patterns for BEfr-SNPs on the face-centered-cubic (FCC), that is, (111), (200), and (220), as well as (311) crystalline planes. This is an indication that the FCC crystalline structure of metallic silver particles corresponded with the Joint Committee on Powder Diffraction Standards (JCPDS no. 00-004-0784, USA) database. Thus, this validated the synthesized silver nanoparticles from BEfr being crystal-like in nature [24]. This evidence is further confirmed by similar patterns of FCC reported from silver nanoparticles synthesized using *Echinochloa stagnina* extract [8]. Concerning the size distribution of BEfr-SNPs determined from the HRTEM micrographs (Figure 5e,f) using image G software, the representative histograms (Figure 5g,h) illustrated that the synthesized BEfr-SNPs at 25 °C as well as 70 °C showed the core size of 19 nm and 18 nm, respectively. These data could imply that BEfr has a higher concentration of capping and reducing agents.

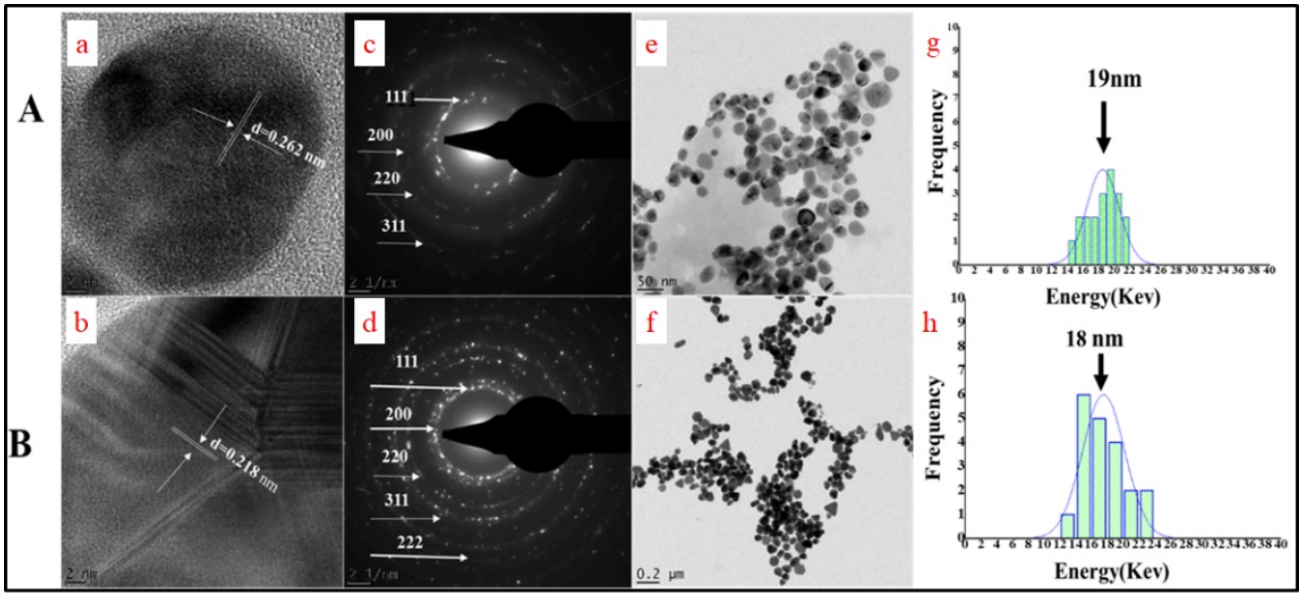

Figure 5. Frequency of diameter and selected area diffraction pattern of BEfr-SNPs. (**A**): BeFr-SNPs-25 °C; (**B**): BEfr-SNPs-70 °C; (**a**,**b**): Silver facet of BEfr-SNPs synthetized at 25 °C and 70 °C; (**c**,**d**): Crystalline planes; (**e**,**f**): Nanostructures; (**g**,**h**): Core size. SAED, selected area electron diffraction; TEM, transmission election microscope.

2.2.4. Energy Dispersive X-ray (EDX) Examination of BEfr-SNPs

The composition of BEfr-SNPs-25 and BEfr-SNPs-70 °C elements were identified using EDX analysis (Figure 6). The biosynthesized BEfr-SNPs EDX profiles revealed the existence of high peaks for elemental silver (Ag^+) at 3 keV, as well as other trace of peaks corresponding to other elements (Figure 6). The distinctive peak of optical absorption at 3 keV is unique to metallic silver nanoparticles because of its SPR [26]. The occurrence of distinctive peaks of C, Cl, and O might be attributed to the components of cellular makeup, such as carbohydrates and proteins derived from the organic matrix, which could have served as a capping agent or stabilizer for the synthesis of SNPs. Indeed, the high oxygen and carbon peaks at 0.5 and 0.0 keV revealed that the compounds of phytochemical that stabilized SNPs are derived from a BEfr extract. Additionally, since the grid is made up of Cu, peaks of other element components, including Cu, were also detected.

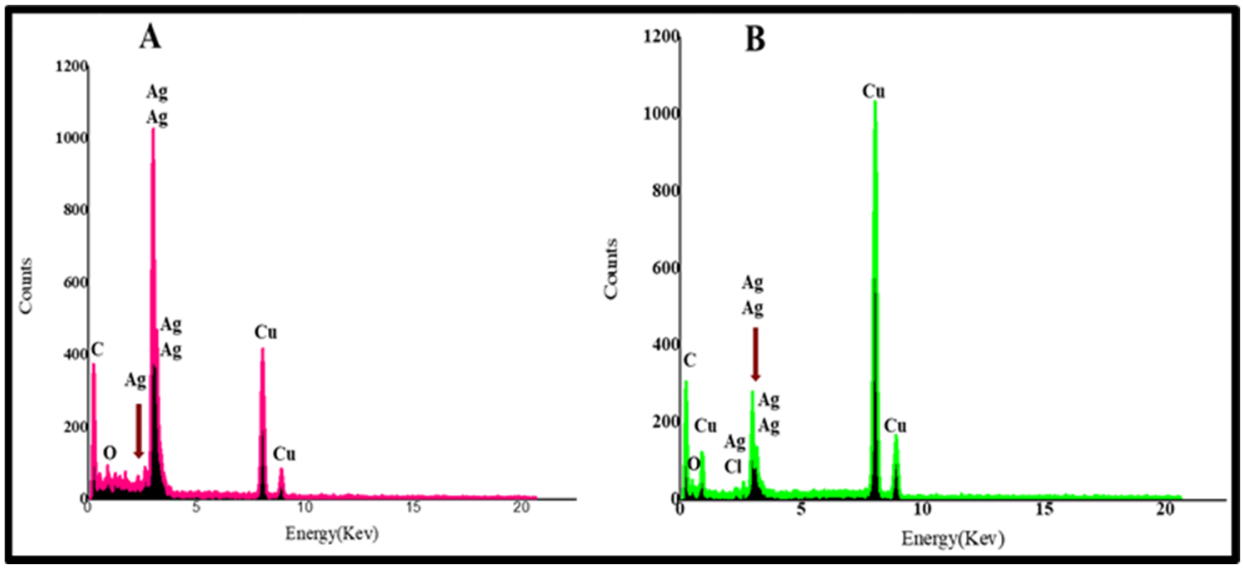

Figure 6. EDX spectra of BEfr-SNPs. (**A**): BEfr-SNPs-25 °C; (**B**): BEfr-SNPs-70 °C. Abbreviations: SNPs, silver nanoparticles; BEfr, fruits from *Bersama engleriana*; EDX, Energy Dispersive X-ray.

2.2.5. Fourier Transform Infrared Spectroscopy (FTIR) Analysis of BEfr-SNPs

FTIR evaluation was used to investigate the putative bonds of functional chemicals obtained from the extracts of BEfr phytochemicals that could be responsible for the capping, reduction, and stability of BEfr-SNPs [7]. The FTIR Spectra of BEfr and BEfr-SNPs are presented in Figure 7 and Table 2. The overall bonds of a chemical recognised in the BEfr extracts as well as BEfr-SNPs include C-H, C-O, –C=C–, O-H, and H–C=O, based on the temperature (25 °C and 70 °C), although some of the peaks were missing in the SNPs. In the IR spectrum of BEfr and BEfr-SNPs, the peaks at 1048 cm^{-1} and 1108 cm^{-1} and 1123 cm^{-1} with the redshift of BEfr and the synthesized BEfr-SNPs at 25 °C and 70 °C, respectively, are characteristic of C=O vibrations of carboxylic acids, esters, and ethers. The identified peaks at 1606.22 cm^{-1} and 1617.28 cm^{-1}, as well as 1606.14 cm^{-1}, showed a redshift of +11.06 and −0.08 cm^{-1} for BEfr and the synthesized BEfr-SNPs at 25 °C and 70 °C, respectively, and correspond to the –C=C– stretch vibration of alkenes. More so, the spectrum at 2016 cm^{-1} may be ascribed to the stretch of –C≡C–alkynes. The stretch wide peaks at 2916.10 cm^{-1}, 2927.29 cm^{-1}, and 2916.16 cm^{-1} of BEfr, BEfr-SNPs-25 °C, and BEfr-SNPs-70 °C, respectively, arises from aldehyde (H–C=O: C–H) stretch vibrations. Furthermore, the observable changes in the band at 3390.07 cm^{-1}, 3401.24 cm^{-1}, and 3401.97 cm^{-1} showed redshifts of +11.1728 cm^{-1} and +11.928 cm^{-1}, in the FTIR spectra of BEfr, BEfr-SNPs-25 °C, and BEfr-SNPs-70 °C respectively, corresponding to the -OH groups found in phenols or alcohol groups.

It has been reported that the possible change in the diverse functional groups is influenced by anthraquinones, flavonoids, saponins, tannins, phenols, and triterpenes present in the BEfr extracts [27], which took part in the capping, reduction, and stability of BEfr-SNPs [8]. These results are in accordance with other results in the literature, which revealed that the stability of plant-based SNPs is due to the amino acids, glycosides, alkaloids, saponins, flavonoids, flavanols, phenols, and polysaccharides present in the plant extract, which function to stabilize the biochemical corona of nanomaterials [7,17,28]. All in all, FTIR spectroscopic evidence revealed that the *Bersama engleriana* extract may perform the dual roles of bioreduction and the stability of the synthesized silver nanoparticle, thereby preventing BEfr-SNPs from adhering and agglomerating. This study is the first to describe the use of *Bersama engleriana* extract as a reducing and stabilizing agent for the synthesis of BEfr-SNPs, to the best of our knowledge.

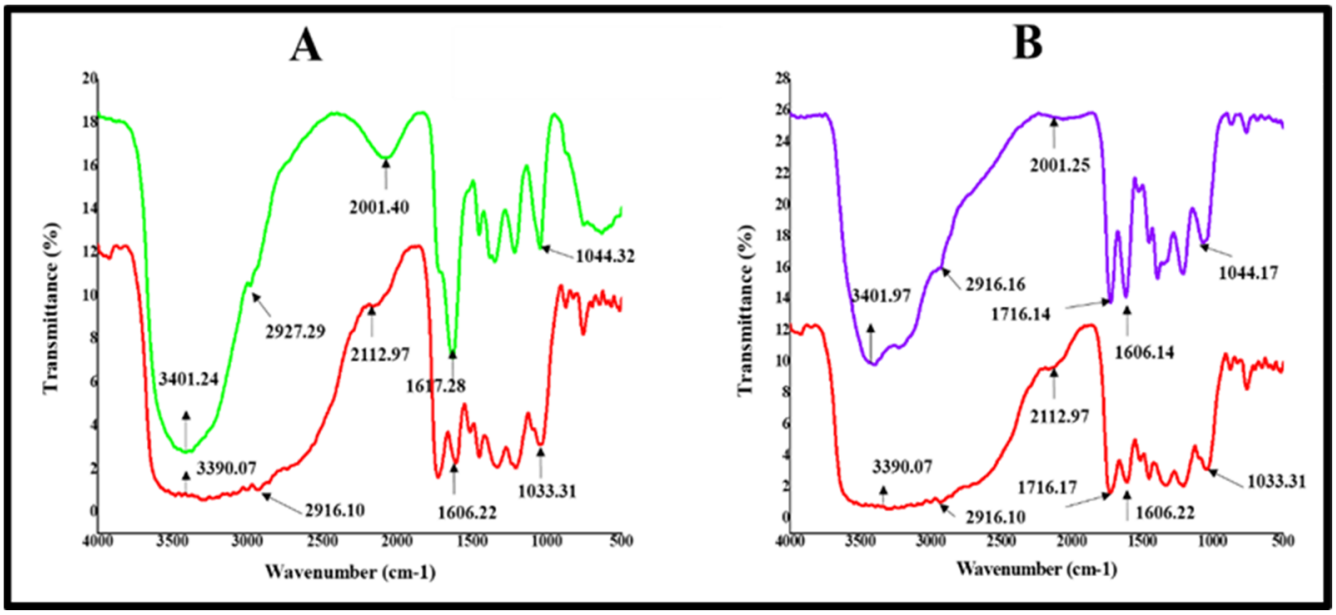

Figure 7. FTIR spectra of BEfr-SNPs compared to the respective BEfr extract. Notes: FTIR spectra of (**A**) BEfr extract (red colour) and BEfr-SNPs synthesized at 25 °C (green colour); (**B**) BEfr extract (red colour) and BEfr-SNPs synthesized at 70 °C (purple colour). Abbreviations: SNPs: Silver nanoparticles; BEfr: fruits from *Bersama engleriana*; FTIR: Fourier transform infrared.

Table 2. FTIR spectra comparison for *Bersama engleriana* extracts and their respective SNPs.

Peak Position in BEfr) (cm^{-1})	Peak Position in SNPs at 25 °C (cm^{-1})	Shift in Position (cm^{-1})	Peak Position in SNPs at 70 °C (cm^{-1})	Shift in Position (cm^{-1})	Type of Chemicals Groups
1033.31	1044.32	+11.03	1044.17	+10.86	C-O carboxylic acids, esters, ethers
1606.22	1617.28	+11.06	1606.14	−0.08	–C=C–stretch alkenes
1716.17	————	———	1716.14	−0.03	C=O Anhydrides
2916.10	2927.29	+11.19	2916.16	+0.06	H–C=O: C–H stretch aldehydes
3390.07	3401.24	+11.17	3401.97	+11.9	O-H, Alcohol, phenol

2.3. Antibacterial Potential of Extracts and Derived Biogenic BEfr-SNPs

The antibacterial effect of *Bersama engleriana* aqueous and methanolic extracts were screened against eight bacterial strains. Initially, the bacteria were treated with 500 µg/mL single dose of *Bersama engleriana* extracts. The antibacterial data in Table 3 demonstrate that the methanolic extract from the fruits of *Bersama engleriana* (BEfrMeOH) was the most effective in terms of MIC values of 125 µg/mL on *Staphylococcus aureus*-NR-45003 and *Salmonella enterica*-NR-4311. However, most of the aqueous extracts of stem bark did not show any efficacy on all the bacteria tested.

Nano-derived products from biosynthesis were tested for antibacterial efficacy in order to overcome multidrug resistance (MDR). The minimum sample concentration required to inhibit visible bacterial growth (MIC) was estimated with the most active extracts (BEfrMeOH) and BEfr-SNPs against thirteen bacteria strains after 24 h of incubation. The MIC values of silver nanoparticles from the fruits of *Bersama engleriana* ranged from 0.234 to >50 µg/mL (Table 4). The silver nanoparticles from the fruits of *Bersama engleriana* (BEfr-SNPs) synthesized at 25 °C were active against seven bacterial strains (*E. coli* ATCC 25922; *S. aureus* NR-45003; *S. enterica* NR-4311; *MRS aureus* ATCC-33591; *K. pneumoniae* ATCC 13883; *S. aureus* NR-48374; and *S. pyogenes* ATCC 19615) with the MICs range of 0.39 to 6.25 µg/mL. The MIC of 0.39 µg/mL was obtained with *E. coli* ATCC 25922, *K. pneumoniae* ATCC 13883, *S. aureus* NR-48374 and *S. pyogenes* ATCC 19615. In addition, the silver nanoparticles from the fruits of *Bersama engleriana* (BEfr-SNPs) synthesized at 70 °C were active with MIC

range of 1.56 to >50 µg/mL against all the bacteria strains tested with *K. pneumoniae* ATCC 13883 having the MIC value of 1.56 µg/mL. A lower value of MIC suggests that fewer therapeutic molecules are required to inhibit the organism's growth; hence, antimicrobial agents with lesser MIC values are more effective [29]. According to some research, SNPs antibacterial activity is more efficient against bacteria, such as *K. pneumoniae* and *S. aureus*, when smaller nanoparticles (<30 nm in size) are employed [30]. The suggested antibacterial activity of SNPs is owed to their small particle size, which provides higher penetration capacity into bacteria, particularly Gram-negative bacteria [5,31].

Table 3. Antibacterial effect of extracts against eight bacterial strains.

Extracts	Microorganism Acronyms							
	A	**B**	**C**	**D**	**E**	**F**	**G**	**H**
BEfrAQ	500	500	500	500	500	500	500	500
BEfrMeOH	500	500	500	500	500	500	125	125
BEfeAQ	500	500	500	500	500	500	500	>500
BEfeMeOH	500	500	500	500	500	500	500	>500
BEeAQ	>500	>500	>500	>500	>500	>500	>500	>500
BEeMeOH	500	>500	500	500	500	500	500	500
Ampicilin	62.5	>62.5	>62.5	>62.5	15.625	62.5	3.901	7.8125

Abbreviations: BEfrAQ: aqueous extract of *Bersama engleriana* fruits; BEfrMeOH: methanolic extract of *Bersama engleriana* fruits; BEfeAQ: aqueous extract of leaves from *Bersama engleriana*; BEfeMeOH: methanolic extract of leaves from *Bersama engleriana*; (BEeAQ): aqueous extract of stem from *Bersama engleriana*; BEeMeOH: methanolic extract of stem from *Bersama engleriana*. (A): *P. aeruginosa* NR-48982: *Pseudomonas aeruginosa* NR-48982; (B): *S. pneumonia* ATCC 49619: *Streptococcus pneumonia* ATCC 49619; (C): *S. enterica* NR-13555: *Salmonella enterica typimurium* NR-13555; (D): *K. pneumoniae: Kpesiella pneumonia* ATCC 700603; (E): *S. aureus* ATCC 43300: *Staphylococcus aureus* ATCC 43300; (F): *E. coli* ATCC 25922: *Eschericha coli* ATCC 25922; (G): *S. aureus* NR-45003; *Staphylococcus aureus* NR-45003; (H): *S. enterica* NR-4311: *Salmonela enterica* NR-4311.

Table 4. Antibacterial effect of bioactive extracts and derived silver nanoparticles against eight bacterial strains.

Acronym	MIC (µg/mL)												
	Bacterial Strains												
	A	**B**	**C**	**D**	**E**	**F**	**G**	**H**	**I**	**K**	**L**	**M**	**N**
BEfrMeOH	500	500	500	500	500	>500	125	125	>500	>500	>500	>500	>500
BEfr-SNPs-25 °C	>50	>50	>50	>50	>50	0.3906	6.25	0.7815	0.7812	0.3906	0.3906	>50	0.3906
BEfr-SNPs-70 °C	> 50	> 50	> 50	> 50	> 50	3.125	> 50	6.25	3.125	1.5612	3.125	> 50	>50
Ampicilin	62.5	>62.5	>62.5	>62.5	15.625	62.5	3.901	7.8125	7.8125	7.8125	3.9062	>62.5	62.50
Ciprofloxacin	0.468	0.468	0.234	0.468	0.234	0.234	0.234	0.234	0.234	0.468	0.234	0.468	0.468

Abbreviations: BEfrMeOH: methanolic extract of fruits from *Bersama engleriana*; (A): *P. aeruginosa* NR-48982: *Pseudomonas aeruginosa* NR-48982; (B): *S. pneumonia* ATCC 49619: *Streptococcus pneumonia* ATCC 49619; (C): *S. enterica* NR-13555: *Salmonella enterica typimurium* NR-13555; (D): *K. pneumoniae* ATCC 700603: *Kpesiella pneumonia* ATCC 700603; (E): *S. aureus* ATCC 43300: *Staphylococcus aureus* ATCC 43300; (F): *E. coli* ATCC 25922: *Eschericha coli* ATCC 25922; (G): *S. aureus* NR-45003: *Staphylococcus aureus* NR-45003; (H): *S. enterica* NR-4311: *Salmonela enterica* NR-4311; (I): *MRS. aureus* ATCC 33591: *Methicilin resistant Staphylococcus aureus* ATCC 33591; (K): *K. pneumoniae* ATCC 13883: *Klebsiella pneumoniae* ATCC 13883; (L): *S. aureus* NR-48374: *Staphylococcus aureus* NR-48374; (M): *S. epidermidis* ATCC 12228: *Staphylococcus epidermidis* ATCC 12228; (N): *S. pyogenes* ATCC 19615: *Streptococcus pyogenes* ATCC 19615.

Several structural factors that could have an effect on the MIC of therapeutic molecules are the solubility of water and polarity, molecular size, dissociation constants, isomers, chemical stability, and functional groups [32]. Generally, BEfr-SNPs produced at 25 °C were the most promising compared to BEfr-SNPs produced at 70 °C. The improved antibacterial activity of SNPs may be due to various factors, such as shape, temperature, and the phytochemicals responsible for capping the SNPs, knowing the FTIR analysis showed the presence of phytochemicals bounds from secondary metabolites [7]. SNPs that have the same surface areas but different shapes exhibit differential bactericidal effects that can

be related to differences in surface area effectiveness, crystallographic surface structures, and active surfaces of SNPs. However, there is little available information on how the nanoparticle shape affects the SNPs biological effect.

2.4. Evaluate the Time Kinetics Effect of Potential Silver Nanoparticles against the Susceptible Bacteria

The growth kinetics of five bacteria strains with the lowest MICs (*E. coli* ATCC 25922, *K. pneumonia* ATCC 13883, *MRS. aureus* ATCC 33591, *S. pyrogenes* ATCC 19615 and *S. aureus* NR-48374) were determined in response to the treatment with the two synthesized BEfr-SNPs as represented in Figure 8. The optical density (OD) changes were employed to ascertain the bacterial growth for 24 h, since this is a fast and simple approach to measure bacterial growth over time. The decline in absorbance suggests bacterial growth inhibition, which could be explained by the cell death inhibited in the stationary phase. Both BEfr-SNPs generated a dose- and time-dependent growth inhibition in the susceptible strains, as shown in Figure 8. The two synthesized BEfr-SNPs (Figure 8) showed a bactericidal effect against the microorganisms until the quarter of the minimal inhibitory concentration; however, the BEfr-SNPs were bacteriostatic at 1/8xMIC. Interestingly, BEfr-SNPs inhibited the development of all five bacterial strains examined. Surprisingly, the growth pattern for *S. pyrogenes* ATCC 19615 demonstrates that ciprofloxacin inhibitory effects, reduce after 4 h and 6 h for BEfr-SNPs-25 °C and BEfr-SNPs-70 °C, respectively. Moreover, a similar effect was obtained in *S. aureus* NR-48374, which showed a decreased effect of ciprofloxacin after 20 h of incubation. In general, Gram-negative bacteria (*E. coli* ATCC 25922 and *K. pneumonia* ATCC 13883) were more sensitive to BEfr-SNPs than Gram-positive bacteria (*S. pyrogenes* ATCC 19615 and *S. aureus* NR-48374). Conversely, the *MRS. aureus* ATCC-33591 was also sensitive to BEfr-SNPs. The difference in sensitivity to SNPs is explained by disparities in the molecular composition and thickness of the membrane structures of Gram-positive and Gram-negative bacteria [33]. Bactericidal activity is believed to be caused by alterations in the cell wall of bacteria structure initiated by interactions with the incorporation of SNPs, resulting in increased membrane permeability and, ultimately, death [34].

Gram-negative bacteria consist of a thinner cell wall that is made up of lipopolysaccharides, phospholipids, and lipoproteins, while the Gram-positive bacteria cell wall has a thick layer of peptidoglycan, teichoic acid that can obstruct nanoparticle penetration [35,36]. Furthermore, Gram-positive bacteria possess a strong negative charge on the surface of the cell wall that can bind SNPs and cause cytoplasmic membrane disruption and, subsequently, cell death [37]. The SNPs antimicrobial activity is generally recognized, although this differs depending on the physical characteristics of the nanoparticle, such as size, shape, and composition, as well as the conditions of synthesis (temperature, pH, and macromolecules) [34]. Their morphologies may be associated with their antibacterial effect, and smaller SNPs have a higher binding surface and exhibit a stronger bactericidal effect compared to larger SNPs [38].

2.5. Evaluate the Effect of Biogenic BEfr-SNPs on Bacteria Cell Membrane of Methicillin-Resistant Staphylococcus aureus

The activity of biogenic SNPs on the outer membrane destabilization of the bacteria was evaluated with *MRSA* bacteria strains, and the destabilization of the membrane by the biogenic SNPs was detected after the treatment with biogenic BEfr-SNPs (Figure 9). The effect of membrane destabilization of the BEfr-SNPs was salt-dependent. As shown in Figure 9, BEfr-SNPs-25 °C at 1MIC, 2MIC, and 4MIC concentrations, affected the growth of bacteria depending on the salt concentration. Interestingly, the increased effect was observed at MIC and 1/2MIC concentrations with a treatment containing NaCl (70%). This depicts the inability of *MRSA* bacteria strains to tolerate NaCl presence in their growth medium. Several studies have documented that the biological effects of SNPs may be attributed to active phytochemicals at specific temperatures [7].

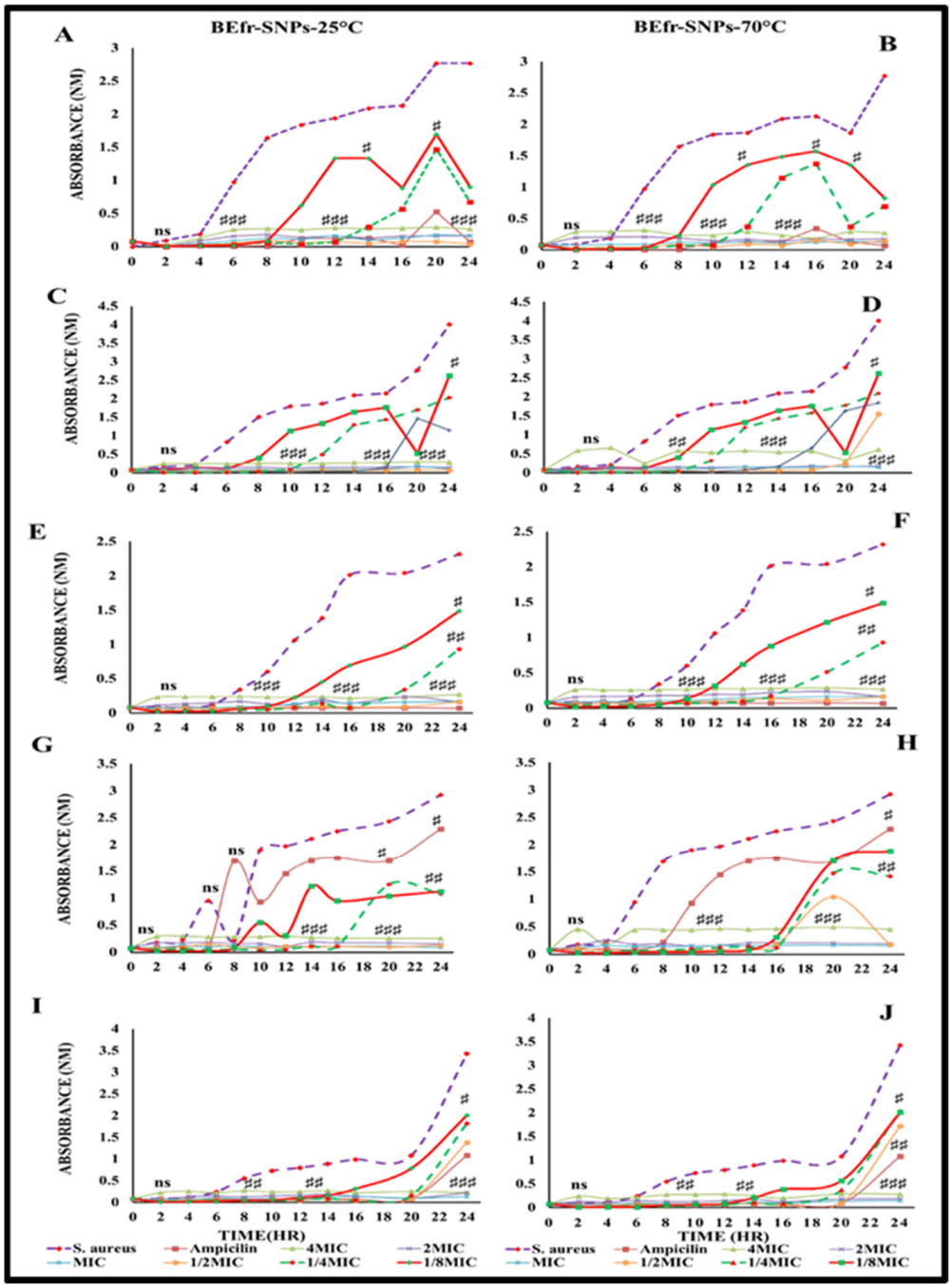

Figure 8. Time-kill kinetics of BEfr-SNPs against selected bacteria strains after 24 h of treatment. $^{\#}$ $p < 0.05$, $^{\#\#}$ $p < 0.01$, $^{\#\#\#}$ $p < 0.001$, significantly different compared to control. The values are represented as means ±SD based on a one-way ANOVA test, then by post hoc multiple comparisons (Tukey's test). Notes: Growth curves of (**A**,**B**): *E. coli* ATCC 25922; (**C**,**D**): *K. pneumonia* ATCC 13883; (**E**,**F**): *MRS. aureus* ATCC 33591; (**G**,**H**): *S. pyrogenes* ATCC 19615; (**I**,**J**): *S. aureus* NR-48374.

The SNPs shape and size also influence NP activity, smaller SNPs is typically more effective since they can readily penetrate across cellular barriers and membrane and impair the physiological processes of bacteria after internalization [39]. Thus, BEfr-SNPs efficacy might be ascribed to their spherical shapes and smaller diameter, because it has been shown that the size of SNPs improves the activity of anti-*MRSA* [40]. The smaller nanoparticle size (19 nm) is very bactericidal and consequently induces membrane destabilization. This implies that the silver nanoparticles with a surface-to-volume ratio provide an inherent specificity for bacteria cell, which possibly facilitates the penetration across the

membrane to get access into the cell. The ionic silver antibacterial effect is associated with its state of valence: with greater-valency, the silver ion Ag (III) displays higher antibacterial characteristics than Ag (I) [40].

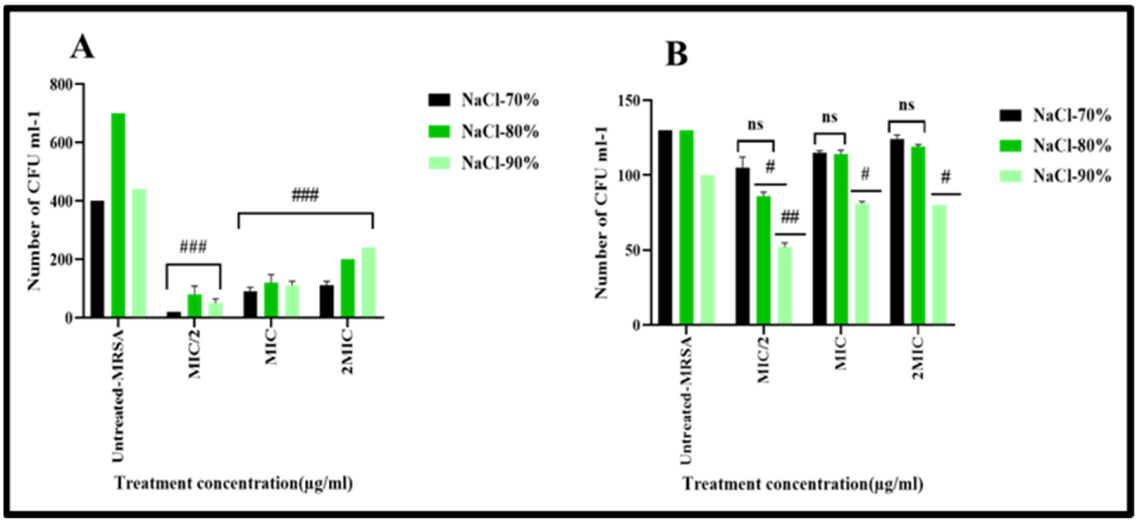

Figure 9. Variation of the number of *MRSA* colonies as a function of the concentration of BEfr-SNPs-25 °C, BEfr-SNPs-70 °C, and NaCl. $^{\#}$ $p < 0.05$, $^{\#\#}$ $p < 0.01$, $^{\#\#\#}$ $p < 0.001$, significantly different compared to control. The values are represented as means ±SD based on a one-way ANOVA test, then by post hoc multiple comparisons (Tukey's test). Abbreviations: *MRS. aureus: Methicilin resistant Staphylococcus aureus*; NaCl: Sodium Chloride.

Additionally, the results could be ascribed to phytochemicals bounds revealed from FTIR (Figure 7), which correlated with extracts from BEfr that are a rich source of polyphenols. For example, tannins and flavonoids have the ability to complex with divalent cations and membrane proteins that result in bacterial membrane destabilization. The low effect observed with BEfr-SNPs synthesized at 70 °C is most likely due to limited concentrations and/or the existence of non-destabilizing particular metabolites of the aforementioned classes caused by the high temperature used in its synthesis. They would almost definitely act through other mechanisms, including intracellular efflux pumps and biofilms, as well as the lysis of cellular proteins or enzymes (*MRSA* penicillinases or ß-lactamases). Many *MRSA* strains, according to the literature, can express large amounts of hydrolytically effective penicillinases (or ß-lactamases), which are proteins that have the ability to hydrolyze ß-lactam drugs to inactive ring-opened derivatives [40]. According to Abbaszadegan et al. [41], when SNPs are exposed to microorganisms, nanoparticles adhere to the cell wall as well as the membrane. The SNPs positive surface charge is critical for adhesion by inducing the electrostatic bond between the negatively charged microorganism cell membranes and SNPs, thereby promoting SNP attachment to cell membranes. Morphological changes occur as a result of such contact and are characterized with shrinking of the cytoplasm as well as the detachment of membrane, which eventually lead to cell wall rupture [42]. In addition, the activity of SNPs could be controlled through the free Ag ions, released or present in the SNPs, which can attach to the cell membrane, disrupt the potential of the membrane, and cause rupture of the bacterial envelope [43,44].

2.6. Determination of the Effect of Bioactive BEfr-SNPs on Nucleotide Leakage

The effect of BEfr-SNPs on DNA nucleotide linkage was evaluated against *MRSA* bacteria strains. As presented in Figure 10, the BEfr-SNPs induced nucleic acids (DNA) release into the extracellular environment, which correlated to nuclear DNA linkage. Indeed, a decrease in OD at 260 nm could turn to a nucleic acid release in the medium

when compared to the growth control. A decline in the OD was observed, meaning that BEfr-SNPs exert their antibacterial activity through this mechanism.

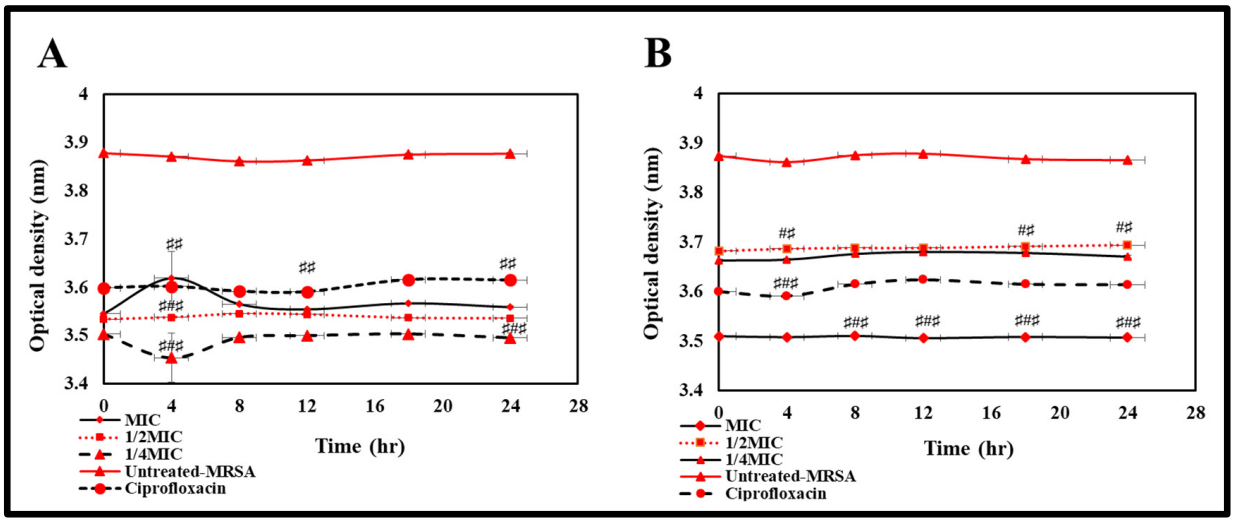

Figure 10. Variation of the optical density as a function of BEfr-SNPs-25 °C and BEfr-SNPs-70 °C with time. $^{\#\#}$ $p < 0.01$, $^{\#\#\#}$ $p < 0.001$, significantly different compared to control. The values are represented as means ±SD based on a one-way ANOVA test, then by post hoc multiple comparisons (Tukey's test). Abbreviations: MIC: Minimum inhibitory concentration, *MRS. aureus: Methicilin resistant Staphylococcus aureus*.

The antimicrobial mechanisms of various flavonoids may be ascribed to the inhibition in the synthesis of nucleic acid because FTIR analysis revealed the availability of phytochemicals bounds that possibly originated from tannins. Indeed, the phytochemicals of extracts from *Bersama engleriana* revealed the presence of tannins, flavonoids, and others [45]. SNPs also bind to the phosphorus- and sulfur-rich biomaterials, which comprise intracellular and extracellular components, including proteins and DNA, as well as membrane proteins. These components have an impact on cell division, respiration, and, ultimately, survival [46]. More so, silver ions, a component of SNPs may enter cells after disrupting the cell wall of bacteria, resulting in the formation and accumulation of DNA damaged, have a great influence on protein synthesis [34,47]. The binding of SNPs with DNA may result in DNA denaturation or shearing, as well as a disruption of cell division [5,48]. Furthermore, SNPs intercalation in the DNA helix could inhibit gene transcription in microorganisms, and SNPs cause DNA molecule modification from relaxed to condensed state, causing a loss of replication ability [47].

Finally, the SNPs binding to *MRSA* bacteria cell membranes and the consequent changes in the lipid bilayer result in enhanced membrane permeability, cell death, and DNA damage, and a strong antibacterial activity that appears to be more significant when nanoparticles with smaller-sized are employed [5]. The findings suggest that the green synthesis of BEfr-SNPs has a significant influence on the optimization of properties and biological effects, as well as the inhibitory efficacy of synthesized BEfr-SNPs, particularly at 25 °C. However, more research is required to improve and gain better insight into the mechanism of antibacterial effect of BEfr-SNPs.

3. Materials and Methods

3.1. Plant Collection and Identification

In December 2015, leaves, fruits, and stem organs of *Bersama engleriana* were collected in Bamendjou, Cameroon, and a voucher specimen (reference: 24725/HNC) was confirmed at the Yaoundé National Herbarium. In this study, the preparation of plant material and the extraction procedure used were previously described by Majoumouo et al., 2020 [49].

3.2. Extraction Procedure

An amount of 100 g of each plant organ powder (leaves, fruits, and stem) was weighed individually into 1000 mL of 100% double-distilled water or methanol for 72 h at 25 °C, with periodic stirring. The generated filtrate solutions were filtered and/or sieved using filter paper (Whatman N° 1). The filtrates were concentrated through a rotary evaporator (Büchi 011, Flawil, Switzerland) at 60 °C (for methanol) under decreased pressure, and the aqueous extracts were lyophilized through the use of a Martin Christ Beta 2–8 lyophilizer (Germany). The concentrates of the methanolic extracts were dried in an open air until consistent weights was attained, and the extract residues were collected and kept at 4 °C for future use.

3.3. Biological Synthesis and Characterization of BEfr-SNPs from Bersama engleriana

The synthesis of the BEfr-SNPs was performed using a previously described method by Majoumouo et al., 2019 [7]. Briefly, the methanolic extracts (50 mg/mL) were prepared in distilled water, and in a 96-well plate, BEfr extracts (50 µL) with concentrations ranging from 0.78 to 50 mg/mL were prepared, followed by the addition of 3 mM $AgNO_3$ (250 µL) to the plant extracts. Duplicate plates were used to prepare the samples, and one of the plates was incubated at 25 °C and the other at 70 °C for 24 h under continuous shaking at 40 rpm. The colour change in the solution was used as an indicator for SNP formation. The optimum extract concentration was selected to upscale NP synthesis to 2 mL with the same conditions. The SNPs were washed thrice with distilled water and centrifuged for 10 min at 14,000× *g* in order to rid of free and unreacted Ag^+ ions and plant extracts. The BEfr-SNPs were resuspended with sterile distilled water and kept at 4 °C for subsequent use. The summary of the SNPs synthesis process is depicted in Figure 11.

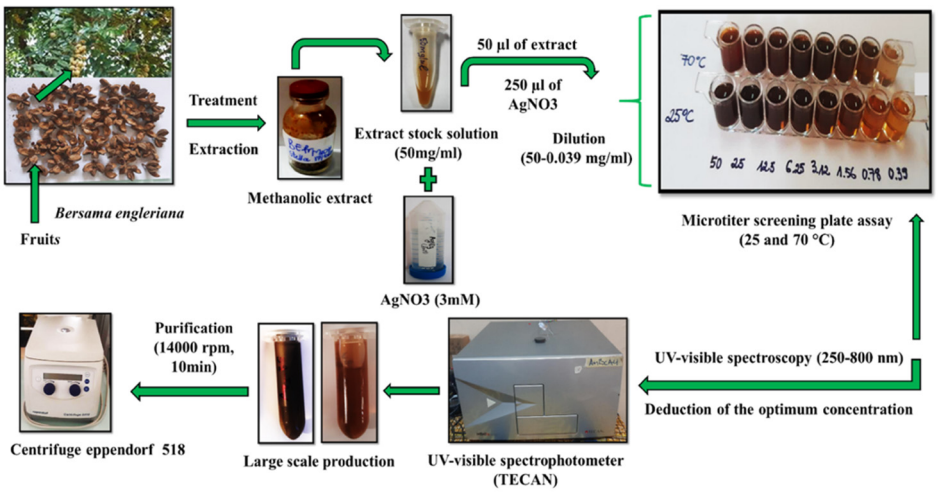

Figure 11. Green synthesis of SNPs from *Bersama engleriana* fruits extracts.

3.4. Characterization of BEfr-SNPs

The SNPs that were synthesized were thoroughly examined using spectroscopy (UV–Vis spectrophotometry and dynamic light scattering (DLS)), energy dispersive X-ray (EDX), selected area diffraction pattern (SAED) as well as Fourier transform infrared (FTIR). Additionally, microscopy (high-resolution transmission election microscopy (HRTEM) methods reported by Majoumouo et al., 2019 [7], with a few modifications was used.

3.4.1. UV–Vis Spectrophotometry Analysis and Dynamic light Scattering (DLS) Analysis

The UV–Vis evaluation of the BEfr-SNPs was carried out using TECAN microplate reader (Infinite M 200, USA), the optical density was measured from 350–700 nm.

The average size and zeta potential, as well as the polydispersity index (Pdi) of the synthesized BEfr-SNPs were analyzed via DLS through the use of a Malvern Nano ZS90 Zetasizer (Malvern, UK).

3.4.2. HRTEM Characterization of BEfr-SNPs

The BEfr-SNPs nanostructure parameters (morphology, core size, and crystallinity) were evaluated using HRTEM under an FEI Tecnai F20, field-emission HRTEM (Oregon, OR, USA) at the Physics and Astronomy Department of the University of the Western Cape. The elemental composition examination was carried out using EDX, and the estimation of materials for elemental and phase determination was performed using SAED assessment. The samples were prepared via the drop-coating a drop of each sample onto a carbon-coated Cu grid. Thereafter, HRTEM was used to evaluate the samples after they had been dried for 10 min under a Xenon light. Transmission electron morphologies were obtained in a bright field mode using a 200 KeV accelerating voltage. An EDX liquid nitrogen cooled Lithium doped Silicon detector was used to collect EDX spectra. The TEM images were analyzed by Image J Software (50b version 1.8.0_60).

3.4.3. Fourier Transform Infrared Spectroscopy (FTIR) Analysis of BEfr-SNPs

FTIR analysis of BEfr-SNPs and extracts were performed. Infrared spectroscopy was done in the Analytical Chemistry Laboratory of the University of Yaoundé I, with the frequency range of 4000 to 400 cm^{-1}. The BEfr-SNPs were dried using a ventilation process, and the BEfr extracts as well as the BEfr-SNPs powders were mixed with the powder of potassium bromide (KBr) and subsequently pressed into a pellet before FTIR evaluation. The baseline adjustments were performed for all spectra using the reference of a blank KBr pellet as a background correction.

3.5. Assessment of In Vitro Antibacterial Effect of BEfr Extracts and BEfr-SNPs

The antibacterial efficacies of the prepared BEfr extracts and BEfr-SNPs derived from methanolic extracts of fruits were tested against thirteen bacterial strains (Table 5) with little modifications from the Clinical Laboratory Standards Institute (CLSI) guidelines [50].

Table 5. List of bacterial strains with their acronyms, reference number, and suppliers.

Bacterial Strains	Acronym	Reference No.	Supplier
Pseudomonas aeruginosa	*P. aeruginosa*	NR-48982	BEI resources
Streptococcus pneumonia	*S. pneumonia*	ATCC 49619	ATCC
Salmonella enterica typhimurium	*S. enterica*	NR-13555	BEI resources
Klebsiella pneumoniae	*K. pneumoniae*	ATCC 700603	ATCC
Staphylococcus aureus	*S. aureus*	ATCC 43300	ATCC
Eschericha coli	*E. coli*	ATCC 25922	ATCC
Staphylococcus aureus	*S. aureus*	NR-45003	BEI resources
Salmonela enterica	*S. enterica*	NR-4311	BEI resources
Methicilin resistant Staphylococcus aureus	*MRS. aureus*	ATCC 33591	ATCC
Klebsiella pneumoniae	*K. pneumoniae*	ATCC 13883	ATCC
Staphylococcusaureus	*S. aureus*	NR-48374	BEI resources
Staphylococcus epidermidis	*S. epidermidis*	ATCC 12228	ATCC
Streptococcus pyogenes	*S. pyogenes*	ATCC 19615	ATCC

3.5.1. Bacterial Strains

The antibacterial activities of SNPs were tested on thirteen bacterial strains. The Research Resources Repository of Biodefense and Emerging Infections (BEI Resources, Rockville, MD 20852) donated some of the bacterial strains, as indicated in Table 5, while others were bought from the American Type Culture Collection (ATCC, Manassas, VA, USA).

3.5.2. Antibacterial Screening of Extracts and Derived Silver Nanoparticles from Bersama engleriana

Single bacterial colonies were inoculated in Mueller–Hinton broth (Sigma, St. Louis, MO, USA), and the cultures were incubated for 24 h at 37 °C with 400 rpm shaking. At 450 nm, the suspensions of the bacteria were standardized to 0.5 McFarland (~1.5×10^8 cells/mL), and each inoculum was diluted to a final concentration of 5×10^5 cells/mL before being dispensed at 100 µL per well in a 96 well plate. BEfr extracts and BEfr-SNPs were tested against thirteen bacterial strains to evaluate whether they had a single point inhibitory effect. To do this end, 100 µL of BEfr (500 µg/mL) or BEfr-SNPs (100 µg/mL) were added separately to wells that contained 100 µL of bacteria and were incubated for 24 h. At 50 µg/mL, ampicillin/ciprofloxacin was used as a positive control, and the visual examination of the bacterial culture turbidity was employed as a bacterial growth indicator.

3.5.3. Evaluation of Minimal Inhibitory Concentration (MIC) of BEfr-SNPs

MICs were determined for Befr-SNPs by using the microdilution test method illustrated above. The bacteria (*P. aeruginosa* NR-48982; *S. pneumonia* ATCC 49619; *S. enterica typimurium* NR-13555; *K. pneumoniae* ATCC 700603; *S. aureus* ATCC 43300; *E. coli* ATCC 25922; *S. aureus* NR-45003; *S. enterica* NR-4311; *MRS aureus* ATCC-33591; *K. pneumoniae* ATCC 13883; *S. aureus* NR-48374; *S. epidermidis* ATCC 12228; and *S. pyogenes* ATCC 19615) were given increasingly higher crude extracts concentrations (0–500 µg/mL) and BEfr-SNPs (0–100 µg/mL). The positive treatment (ciprofloxacin and ampicillin at 0–50 µg/mL) and negative (untreated) controls were also incorporated into the testing groups. The bacterial suspension turbidity was visually examined after 24 h of treatment as an indicator of bacterial growth. The smallest concentration that inhibited the observed bacterial growth was obtained as the MIC. All tests were carried out in triplicate.

3.5.4. Study of Bacterial Time Kill Growth Inhibition of Active BEfr-SNPs

The time-killing kinetics of BEfr-SNPs was estimated following the method illustrated by Cao et al., 2012 [51], with few modifications. The assay was done in triplicate and the silver nanoparticles solution concentrated at 1MIC, 1/2MIC, 1/4MIC, and 1/8MIC were prepared through serial twofold dilution in a 96-well microplate. An amount of 100 µL of bacterial suspension (1.5×10^6 CFU/mL) was introduced into each well of the microplate. The bacterial cultures OD was evaluated at 630 nm at different time intervals (2, 4, 6, 8, 10, 12, 14,16,18, 20, and 24 h) to monitor the growth rate of the bacteria, and the absorbance (OD 630 nm) against time (hours) growth curves was plotted.

3.5.5. Analysis of the Effect of Extraction on Membrane Destabilization Using Loss of Salt Tolerance Assay

The ability of *Methicilin-Resistant Staphylococcus aureus* to grow colonies on NaCl-supplemented MHA in the presence of extracts was examined using the method previously described by Etame et al., 2018 [52]. Indeed, a preliminary assessment was performed by cultivating *MRSA* bacteria for 24 h at 37 °C on a supplement of MHA with NaCl at various concentrations (10–100 mg/mL). The number of colonies was counted at the end of the incubation time, and the concentrations of NaCl that had no effect on the bacterial growth were selected. Thereafter, BEfr-SNPs at various concentrations (1MIC, 2MIC, and 4MIC) were mixed with the cells (0.5 McFarland) and incubated for 1 h at 37 °C. Subsequently, each well contents were subcultured on MHA enriched with NaCl at specific concentrations (60, 70, and 80 mg/mL). The petri dishes were incubated for 24 h at 37 °C, while the colony-forming units (CFU) number was plotted against the concentrations of silver nanoparticles and NaCl. The tests were carried out in triplicate.

3.5.6. Analysis of the Effect of Bioactive BEfr-SNPs on Nucleotide Leakage

The experiment was performed in accordance with the method previously described by Oliveira et al., 2015 [53]. Briefly, an *Methicilin resistant Staphylococcus aureus* overnight

culture was washed in sterile physiologic water (2 mL of 0.9% NaCl), and the resultant solution was centrifuged for 10 min at 10,000× *g*. Subsequently, the supernatant was removed, and the pellet was resuspended in 10 mM PBS (pH 7.4) with the turbidity adjusted to 0.5 McFarland (1.5×10^8 CFU/mL). The inoculum (100 µL) was added to 100 µL of MHB with varying concentrations of silver nanoparticle solutions (1MIC, 2MIC, 4MIC) and incubated at various time points (0, 2, 4, 6, 8, and 12 h). After each incubation time, the suspension of cell was centrifuged for 10 min at 10,000× *g*, the supernatant was diluted accordingly, and OD at 260 nm were measured. Negative control (PBS + cell suspension), positive control (ciprofloxacin), blank (MHB + Silver nanoparticle solution), and sterility control (MHB alone) tests were performed in triplicate and concurrently. The ODs of the various extract concentrations were plotted against time to measure the degree of leakage as a time-dependent.

3.6. Statistical Analysis

Graph Pad Prism version 8.0.0 for Windows, Graph Pad Software, San Diego, CA, USA, www.graphpad.com (accessed on 13 June 2022), was used to analyze the results. The values are represented as means ± SD based on a one-way ANOVA test, then by post hoc multiple comparisons (Tukey's test). A *p*-value of <0.05 was considered statistically significance and denoted with an asterisk ($^{\#}$). $^{\#}$ $p < 0.05$, $^{\#\#}$ $p < 0.01$, $^{\#\#\#}$ $p < 0.001$.

4. Conclusions

This study is the first to describe silver nanoparticle synthesis from methanolic extracts of *Bersama engleriana* with HRTEM sizes of 18 and 19 nm. The silver nanoparticles produced at 25 °C were spherical in shapes and exhibited powerful antibacterial activity with a decrease of MIC at more than 30 folders compared to the extracts against the tested pathogenic bacteria. The findings revealed that biogenic nanoparticles exhibited significant bactericidal effects. Interestingly, the mode of action of the silver nanoparticles produced at 25 °C was attained through the outer membrane destabilization of *MRSA* bacteria strains and/or through the prevention of the expulsion of salt from the bacterial cells, as well as DNA nucleotide linkage. This evidence showed that the silver nanoparticles from *Bersama engleriana*, through their bactericidal effects, could be a new hope in the development of antibacterial drugs. Further studies are underway to extend the study on other microorganisms and evaluate the mechanism of silver nanoparticles from *Bersama engleriana* on biofilm formation, the inhibition of efflux pumps cellular protein, and others.

Author Contributions: Conceptualization, M.S.M., M.B.T., Y.D.Y., F.F.B. and T.M.; methodology, M.S.M., M.B.T., Y.D.Y. and T.M.; validation, M.S.M., M.B.T., T.A.A., F.F.B. and T.M.; formal analysis, M.S.M., M.B.T., Y.D.Y., F.F.B. and T.M.; investigation, M.S.M. and M.B.T.; resources, M.B.T., F.F.B., R.T.A., N.A. and T.M.; data curation, M.B.T., F.F.B. and T.M.; writing—original draft preparation, M.S.M. and M.B.T.; writing—review and editing, M.S.M., M.B.T., Y.D.Y., T.A.A., R.T.A., N.A., F.F.B. and T.M.; visualization, M.S.M., M.B.T., T.A.A. and T.M.; supervision, M.B.T., F.F.B. and T.M.; project administration, M.S.M. and M.B.T.; funding acquisition, M.B.T., F.F.B., R.T.A., N.A., F.F.B. and T.M. All authors have read and agreed to the published version of the manuscript.

Funding: This research was funded by the South African Department of Science and Technology and the National Research Foundation (DST/NRF) Innovation Postdoctoral Fellowship supported by the South African Ministry of Research and Innovation (Grant No: 116622) to MBT. The APC was funded by R.T.A., N.A. and the University of the Western Cape Research Office.

Institutional Review Board Statement: Not applicable.

Informed Consent Statement: Not applicable.

Data Availability Statement: The data that support the findings of this article are openly available at PubMed (https://pubmed.ncbi.nlm.nih.gov/, accessed on 13 June 2022).

Acknowledgments: The authors are thankful for the material and equipment received from the Food Toxicology Laboratory, Department of Medical Bioscience, University of the Western Cape;

from the Yaoundé-Bielefeld Bilateral Graduate School for Natural Products with Anti-Parasite and Antibacterial Activity (YaBiNaPA); and the Seeding Labs' Instrumental Access.

Conflicts of Interest: The authors declare no conflict of interest.

References

1. Nkengasong, J.N.; Tessema, S.K. Africa Needs a New Public Health Order to Tackle Infectious Disease Threats. *Cell* **2020**, *183*, 296–300. [CrossRef]
2. Gajdács, M.; Urbán, E.; Stájer, A.; Baráth, Z. Antimicrobial Resistance in the Context of the Sustainable Development Goals: A Brief Review. *Eur. J. Investig. Health Psychol. Educ.* **2021**, *11*, 71–82. [CrossRef]
3. Centers for Disease Control and Prevention (CDC). *National Center for Emerging and Zoonotic Infectious Diseases (NCEZID) Progress Report, Protecting Health in 2020*; CDC: Atlanta, GA, USA, 2020.
4. Tincho, M.; Morris, T.; Meyer, M.; Pretorius, A. Antibacterial Activity of Rationally Designed Antimicrobial Peptides. *Int. J. Microbiol.* **2020**, *2020*, 2131535. [CrossRef]
5. Dakal, T.C.; Kumar, A.; Majumdar, R.S.; Yadav, V. Mechanistic basis of antimicrobial actions of silver nanoparticles. *Front. Microbiol.* **2016**, *7*, 1831. [CrossRef]
6. Baptista, P.V.; McCusker, M.P.; Carvalho, A.; Ferreira, D.A.; Mohan, N.M.; Martins, M.; Fernanades, A.R. Nano-Strategies to Fight Multidrug Resistant Bacteria—"A Battle of the Titans". *Front. Microbiol.* **2018**, *9*, 1441. [CrossRef]
7. Majoumouo, M.S.; Sibuyi, N.R.S.; Tincho, M.B.; Mbekou, M.; Boyom, F.F.; Meyer, M. Enhanced Anti-Bacterial Activity of Biogenic Silver Nanoparticles Synthesized from Terminalia mantaly Extracts. *Int. J. Nanomed.* **2019**, *14*, 9031–9046. [CrossRef]
8. Shehabeldine, A.M.; Elbahnasawy, M.A.; Hasaballah, A.I. Green Phytosynthesis of Silver Nanoparticles Using Echinochloa stagnina Extract with Reference to Their Antibacterial, Cytotoxic, and Larvicidal Activities. *BioNanoScience* **2021**, *11*, 526–538. [CrossRef]
9. Singh, P.; Garg, A.; Pandit, S.; Mokkapati, V.R.S.S.; Mijakovic, I. Antimicrobial Effects of Biogenic Nanoparticles. *Nanomaterials* **2018**, *8*, 1009. [CrossRef] [PubMed]
10. Backx, B.P.; dos Santos, M.S.; dos Santos, O.A.; Filho, S.A. The Role of Biosynthesized Silver Nanoparticles in Antimicrobial Mechanisms. *Curr. Pharm. Biotechnol.* **2021**, *22*, 762–772. [CrossRef]
11. Shankar, S.S.; Rai, A.; Ankamwar, B.; Singh, A.; Ahmad, A.; Sastry, M. Biological synthesis of triangular gold nanoprisms. *Nat. Mater.* **2004**, *3*, 482–488. [CrossRef]
12. Singh, P.; Ahn, S.; Kang, J.-P.; Veronika, S.; Huo, Y.; Singh, H.; Chokkaligam, M.; Farh, M.E.-A.; Aceituno, V.C.; Kim, Y.J.; et al. In vitro anti-inflammatory activity of spherical silver nanoparticles and monodisperse hexagonal gold nanoparticles by fruit extract of *Prunus serrulata*: A green synthetic approach. *Artif. Cells Nanomed. Biotechnol.* **2018**, *46*, 2022–2032. [CrossRef]
13. Singh, A.; Jain, D.; Upadhyay, M.K.; Khandelwal, N.; Verma, H.N. Green Synthesis of Silver Nanoparticles Using Argemone Mexicana Leaf Extract and Evaluation of Their Anti-microbial Activities. *Dig. J. Nanomater. Biostruct.* **2010**, *5*, 483–489.
14. Anuj, S.A.; Gajera, H.; Hirpara, D.G.; Golakiya, B.A. Bacterial membrane destabilization with cationic particles of nano-silver to combat efflux-mediated antibiotic resistance in Gram-negative bacteria. *Life Sci.* **2019**, *230*, 178–187. [CrossRef]
15. Boateng, J.; Catanzano, O. *Silver and Silver Nanoparticle-Based Antimicrobial Dressings. Therapeutic Dressings and Wound Healing Applications*; John Wiley and Sons: Hoboken, NJ, USA, 2020; Chapter 8; pp. 157–184. [CrossRef]
16. Burdușel, A.-C.; Gherasim, O.; Grumezescu, A.M.; Mogoantă, L.; Ficai, A.; Andronescu, E. Biomedical Applications of Silver Nanoparticles: An Up-to-Date Overview. *Nanomaterials* **2018**, *8*, 681. [CrossRef] [PubMed]
17. Das, G.; Shin, H.-S.; Kumar, A.; Vishnuprasad, C.N.; Patra, J.K. Photo-mediated optimized synthesis of silver nanoparticles using the extracts of outer shell fibre of Cocos nucifera L. fruit and detection of its antioxidant, cytotoxicity and antibacterial potential. *Saudi J. Biol. Sci.* **2020**, *28*, 980–987. [CrossRef] [PubMed]
18. Dakshayani, S.S.; Marulasiddeshwara, M.B.; Sharath Kumar, M.N.; Ramesh, G.; Kumar, R.; Devaraja, S.; Hosamani, R. Antimicrobial, anticoagulant and antiplatelet activities of green synthesized silver nanoparticles using Selaginella (Sanjeevini) plant extract. *Int. J. Biol. Macromol.* **2019**, *131*, 787–797.
19. Sengupta, A.; Sarkar, A. Synthesis and characterization of nanoparticles from neem leaves and banana peels: A green prospect for dye degradation in wastewater. *Ecotoxicology* **2021**, *31*, 537–548. [CrossRef]
20. Hiemenz, P.C.; Rajagopalan, R. *Principles of Colloid and Surface Chemistry, Revised and Expanded*; CRC Press: Boca Raton, FL, USA, 2016.
21. El-Desouky, N.; Shoueir, K.R.; El-Mehasseb, I.; El-Kemary, M. Bio-inspired green manufacturing of plasmonic silver nanoparticles/Degussa using Banana Waste Peduncles: Photocatalytic, antimicrobial, and cytotoxicity evaluation. *J. Mater. Res. Technol.* **2020**, *10*, 671–686. [CrossRef]
22. Ahmad, A.; Syed, F.; Shah, A.; Khan, Z.; Tahir, K.; Khan, A.U.; Yuan, Q. Silver and gold nanoparticles from Sargentodoxa cuneata: Synthesis, characterization and antileishmanial activity. *RSC Adv.* **2015**, *5*, 73793–73806. [CrossRef]
23. Kumar, K.M.; Sinha, M.; Mandal, B.K.; Ghosh, A.R.; Kumar, K.S.; Reddy, P.S. Green synthesis of silver nanoparticles using Terminalia chebula extract at room temperature and their antimicrobial studies. *Spectrochim. Acta Part A Mol. Biomol. Spectrosc.* **2012**, *91*, 228–233. [CrossRef]

24. Bagherzade, G.; Tavakoli, M.M.; Namaei, M.H. Green synthesis of silver nanoparticles using aqueous extract of saffron (*Crocus sativus* L.) wastages and its antibacterial activity against six bacteria. *Asian Pac. J. Trop. Biomed.* **2017**, *7*, 227–233. [CrossRef]
25. Guo, Y.; Sun, Q.; Wu, F.-G.; Dai, Y.; Chen, X. Polyphenol-Containing Nanoparticles: Synthesis, Properties, and Therapeutic Delivery. *Adv. Mater.* **2021**, *33*, 2007356. [CrossRef] [PubMed]
26. Galvez, A.M.; Ramos, K.M.; Teja, A.J.; Baculi, R. Bacterial Exopolysaccharide-Mediated Synthesis of Silver Nanoparticles and Their Application on Bacterial Biofilms. *J. Microbiol. Biotechnol. Food Sci.* **2019**, *8*, 970–978. [CrossRef]
27. Kuete, V.; Mbaveng, A.T.; Tsaffack, M.; Beng, V.P.; Etoa, F.-X.; Nkengfack, A.E.; Meyer, J.M.; Lall, N. Antitumor, antioxidant and antimicrobial activities of Bersama engleriana (Melianthaceae). *J. Ethnopharmacol.* **2008**, *115*, 494–501. [CrossRef]
28. Okaiyeto, K.; Hoppe, H.; Okoh, A.I. Plant-Based Synthesis of Silver Nanoparticles Using Aqueous Leaf Extract of Salvia officinalis: Characterization and its Antiplasmodial Activity. *J. Clust. Sci.* **2020**, *32*, 101–109. [CrossRef]
29. Emani, S.; Gunjiganur, G.V.; Mehta, D.S. Determination of the antibacterial activity of simvastatin against periodontal pathogens, Porphyromonas gingivalis and Aggregatibacter actinomycetemcomitans: An in vitro study. *Contemp. Clin. Dent.* **2014**, *5*, 377–382. [CrossRef]
30. Collins, T.L.; Markus, E.A.; Hassett, D.J.; Robinson, J.B. The Effect of a Cationic Porphyrin on Pseudomonas aeruginosa Biofilms. *Curr. Microbiol.* **2010**, *61*, 411–416. [CrossRef]
31. Morones, J.R.; Elechiguerra, J.L.; Camacho, A.; Holt, K.; Kouri, J.B.; Ramírez, J.T.; Yacaman, M.J. The bactericidal effect of silver nanoparticles. *Nanotechnology* **2005**, *16*, 2346–2353. [CrossRef]
32. Van De Vel, E.; Sampers, I.; Raes, K. A review on influencing factors on the minimum inhibitory concentration of essential oils. *Crit. Rev. Food Sci. Nutr.* **2017**, *59*, 357–378. [CrossRef]
33. Kim, J.S.; Kuk, E.; Yu, K.N.; Kim, J.-H.; Park, S.J.; Lee, H.J.; Kim, S.H.; Park, Y.K.; Park, Y.H.; Hwang, C.-Y.; et al. Antimicrobial effects of silver nanoparticles. *Nanomed. Nanotechnol. Biol. Med.* **2007**, *3*, 95–101. [CrossRef]
34. Chung, I.-M.; Park, I.; Seung-Hyun, K.; Thiruvengadam, M.; Rajakumar, G. Plant-Mediated Synthesis of Silver Nanoparticles: Their Characteristic Properties and Therapeutic Applications. *Nanoscale Res. Lett.* **2016**, *11*, 40. [CrossRef] [PubMed]
35. Kumarasinghe, K.G.U.R.; Silva, W.C.H.; Fernando, M.D.A.; Palliyaguru, L.; Jayawardena, P.S.; Shimomura, M.; Fernando, S.S.N.; Gunasekara, T.D.C.P.; Jayaweera, P.M. One-Pot Reducing Agent-Free Synthesis of Silver Nanoparticles/Nitrocellulose Composite Surface Coating with Antimicrobial and Antibiofilm Activities. *BioMed Res. Int.* **2021**, *2021*, 6666642. [CrossRef] [PubMed]
36. Permana, A.D.; Anjani, Q.K.; Sartini; Utomo, E.; Volpe-Zanutto, F.; Paredes, A.J.; Evary, Y.M.; Mardikasari, S.A.; Pratama, M.R.; Tuany, I.N.; et al. Selective delivery of silver nanoparticles for improved treatment of biofilm skin infection using bacte-ria-responsive microparticles loaded into dissolving microneedles. *Mater. Sci. Eng. C* **2021**, *120*, 111786. [CrossRef]
37. Wang, L.; Hu, C.; Shao, L. The antimicrobial activity of nanoparticles: Present situation and prospects for the future. *Int. J. Nanomed.* **2017**, *12*, 1227–1249. [CrossRef]
38. Kvitek, D.J.; Will, J.L.; Gasch, A.P. Variations in Stress Sensitivity and Genomic Expression in Diverse S. cerevisiae Isolates. *PLoS Genet.* **2008**, *4*, e1000223. [CrossRef] [PubMed]
39. Aljabali, A.A.A.; Akkam, Y.; Al Zoubi, M.S.; Al-Batayneh, K.M.; Al-Trad, B.; Alrob, O.A.; Alkilany, A.M.; Benamara, M.; Evans, D.J. Synthesis of Gold Nanoparticles Using Leaf Extract of Ziziphus zizyphus and their Antimicrobial Activity. *Nanomaterials* **2018**, *8*, 174. [CrossRef] [PubMed]
40. Labruère, R.; Sona, A.J.; Turos, E. Anti–Methicillin-Resistant Staphylococcus aureus Nanoantibiotics. *Front. Pharmacol.* **2019**, *10*, 1121. [CrossRef]
41. Abbaszadegan, A.; Ghahramani, Y.; Gholami, A.; Hemmateenejad, B.; Dorostkar, S.; Nabavizadeh, M.; Sharghi, H. The Effect of Charge at the Surface of Silver Nanoparticles on Antimicrobial Activity against Gram-Positive and Gram-Negative Bacteria: A Preliminary Study. *J. Nanomater.* **2015**, *2015*, 53. [CrossRef]
42. Nalwade, A.R.; Jadhav, A.A. Biosynthesis of silver nanoparticles using leaf extract of Daturaalba Nees. and evaluation of their antibacterial activity. *Arch. Appl. Sci. Res.* **2013**, *5*, 45–49.
43. Bapat, R.A.; Chaubal, T.V.; Joshi, C.P.; Bapat, P.R.; Choudhury, H.; Pandey, M.; Gorain, B.; Kesharwani, P. An overview of application of silver nanoparticles for biomaterials in dentistry. *Mater. Sci. Eng. C* **2018**, *91*, 881–898. [CrossRef]
44. Yin, I.X.; Zhang, J.; Zhao, I.S.; Mei, M.L.; Li, Q.; Chu, C.H. The Antibacterial Mechanism of Silver Nanoparticles and Its Application in Dentistry. *Int. J. Nanomed.* **2020**, *15*, 2555–2562. [CrossRef] [PubMed]
45. Majoumouo, M.S.; Tincho, M.B.; Morris, T.; Hiss, D.C.; Boyom, F.F.; Mandal, C. Antiproliferative potential of methanolic and aqueous extracts and their methanolic fractions derived from fruits of Bersama engleriana against a panel of four cancer cell lines. *Cogent Biol.* **2020**, *6*, 1727636. [CrossRef]
46. Song, H.Y.; Ko, K.K.; Oh, I.H.; Lee, B.T. Fabrication of Silver Nanoparticles and Their Antimicrobial Mechanisms. *Eur. Cells Mater.* **2006**, *11*, 58–59.
47. Feng, Q.L.; Wu, J.; Chen, G.Q.; Cui, F.Z.; Kim, T.N.; Kim, J.O. A mechanistic study of the antibacterial effect of silver ions onEscherichia coli and Staphylococcus aureus. *J. Biomed. Mater. Res.* **2000**, *52*, 662–668. [CrossRef]
48. Kumar, N.; Das, S.; Jyoti, A.; Kaushik, S. Synergistic effect of silver nanoparticles with doxycycline against Klebsiella pneumoniae. *Int. J. Pharm. Pharm. Sci.* **2016**, *8*, 183–186.
49. Majoumouo, M.S.; Sharma, J.R.; Sibuyi, N.R.S.; Tincho, M.B.; Boyom, F.F.; Meyer, M. Synthesis of Biogenic Gold Nanoparticles from *Terminalia mantaly* Extracts and the Evaluation of Their In Vitro Cytotoxic Effects in Cancer Cells. *Molecules* **2020**, *25*, 4469. [CrossRef]

50. Clinical Laboratory Standard Institute. *Methods for Dilution Antimicrobial Susceptibility Tests for Bacteria that Grow Aerobically; Approved Standard-Ninth Edition Document, Replaces M07-A8*; Clinical Laboratory Standard Institute: Wayne, PA, USA, 2012; Volume 29, p. 2.
51. Ho, P.L.; Cao, L.; Dai, C.; Li, Z.; Fan, Z.; Song, Y.; Wu, Y.; Cao, Z.; Li, W. Antibacterial Activity and Mechanism of a Scorpion Venom Peptide Derivative In Vitro and In Vivo. *PLoS ONE* **2012**, *7*, e40135.
52. Etame, R.E.; Mouokeu, R.S.; Pouaha, C.L.C.; Kenfack, I.V.; Tchientcheu, R.; Assam, J.P.A.; Poundeu, F.S.M.; Tiabou, A.T.; Etoa, F.X.; Kuiate, J.R.; et al. Effect of Fractioning on Antibacterial Activity of *Enantia chlorantha* Oliver (Annonaceae) Methanol Extract and Mode of Action. *Evid. Based Complement. Altern. Med.* **2018**, *2018*, 4831593. [CrossRef]
53. Oliveira, D.M.; Melo, F.G.; Balogun, S.O.; Flach, A.; de Souza, E.C.A.; de Souza, G.P.; Rocha, I.D.N.A.; da Costa, L.A.M.A.; Soares, I.M.; da Silva, L.I.; et al. Antibacterial mode of action of the hydroethanolic extract of *Leonotis nepetifolia* (L.) R. Br. involves bacterial membrane perturbations. *J. Ethnopharmacol.* **2015**, *172*, 356–363. [CrossRef]